PAPER • OPEN ACCESS

Design and experimental set-up of hydrogen based microgrid: characterization of components and control system development

To cite this article: Carmine Cava *et al* 2022 *J. Phys.: Conf. Ser.* **2385** 012042

View the article online for updates and enhancements.

Design and experimental set-up of hydrogen based microgrid: characterization of components and control system development

Carmine Cava[1]**, Carlotta Cosentini**[1]**, Gabriele Guglielmo Gagliardi**[2]**, Luca Cedola**[2]**, Michele Vincenzo Migliarese Caputi**[2]**, Marco Aresti**[3] **and Domenico Borello**[2]

[1] Department of Astronautical, Electrical and Energy Engineering, Sapienza University of Rome, Rome, Italy
[2] Department of Mechanical and Aerospace Engineering, Sapienza University of Rome, Rome, Italy
[3] REN-O&M, Enel Green Power S.p.A., Rome, Italy

E-mail: `carmine.cava@uniroma1.it`

Abstract. In this study, the implementation of a hydrogen microgrid is investigated, considering the integration of H_2 production, storage, and energy conversion to feed a typical end-user. A remote control system has been realized through LabVIEW software, allowing to monitor real-time all the devices and analyze their performances. The integrated system is composed of a PEM electrolyzer ($325\,W$), a storage system based on metal hydrides (two tanks, $54\,g$ of hydrogen each, $1.08\,wt\%$) and an energy converter (PEM Fuel Cell stack, $200\,W$). A programmable electronic load was used to set a power demand throughout the year, simulating an end-user. Data collected from each component of the micro-grid were used to characterize the energetic performance of the devices, focusing on the H_2 production via electrolyzer, charging cycles of the H_2 storage system, and energy conversion efficiency of the FC stack. Finally, the global efficiency of the microgrid is computed. Even though the system is realized in laboratory scale, this circumstance will not invalidate the significance of the configuration due to modularity of all the technologies that can be easily scaled up to realistic scales.

1. Introduction

Hydrogen technologies are attracting the attention of world population because they can be used to overcome the issue related to the intermittency of the renewable energy sources (RES) commonly used, such as solar and wind. Hydrogen is energetically very appealing because is the molecule with the highest energy content by weight ($120 \div 143\,MJ/kg$) [1]. Hydrogen is mainly produced by water electrolysis. If the electricity to run the process derives from RES, like wind or solar, the hydrogen is completely "green". Hydrogen can be stored in several ways (physical storage, such as liquid and compressed, and chemical storage in metal hydrides) and can be used to feed fuel cells for power generation, fuel for transport sector as well as chemical for hard-to abate sector [2]. Respect to conventional energy storage systems like batteries and supercapacitors, hydrogen technologies have slow response time but high energy density giving superior autonomy to the system [3]. Additionally, even though safety issues are present due to the risk of explosion, hydrogen is not toxic as the typical lithium-ion battery acid chemistries

used today. Hence, the modern microgrids with hybrid battery-hydrogen systems represent a valuable solution to increase the penetration of RES into the energy mix.

An intelligent and integrated control system between each component is an essential requirement for the feasibility and reliability of these systems [4]. Some experimental projects have been carried out until, for example Cau et al [5] have modeled and simulated an isolated hybrid micro-grid with hydrogen production and storage. A real plant for production and storage of hydrogen produced from wind energy was demonstrated at Utsira in Norway [6]. Although these projects demonstrated the autonomy and safety of the hydrogen systems, there are many missing data that must be considered for a proper system optimization. To get a complete view of the overall system performance and to develop the proper control strategies, it is necessary to characterize each equipment before integration [7]. The main controller can then consider all the constraints, limitations, degradation issues of each energy storage systems (ESS) and estimate the real performance.

The objective of this research activity is to implement, monitor and characterize a hydrogen-based ESS to be used in a micro-grid to feed a typical end-user. The integrated system is composed of a PEM water electrolyzer, a storage system based on metal hydrides, a stack of PEM Fuel Cell and a lead acid battery bank. A programmable electronic load was used to set a power demand by simulating an end-user. A remote monitoring and measurement station was realized with LabVIEW software, allowing to check real-time some operating parameters of the connected devices and analyze their performances. The data collected allowed to characterize the devices and provided important indications for the development of the control system. This procedure will support a rapid testing and validation of alternative devices by developing a system able to use the output of any component to support an optimal operation of micro-grid. Even though the scales are small compared to real applications, this circumstance will not invalidate the significance of the configuration provided that all the devices will be scaled accordingly and that the difference in efficiency can be properly estimated.
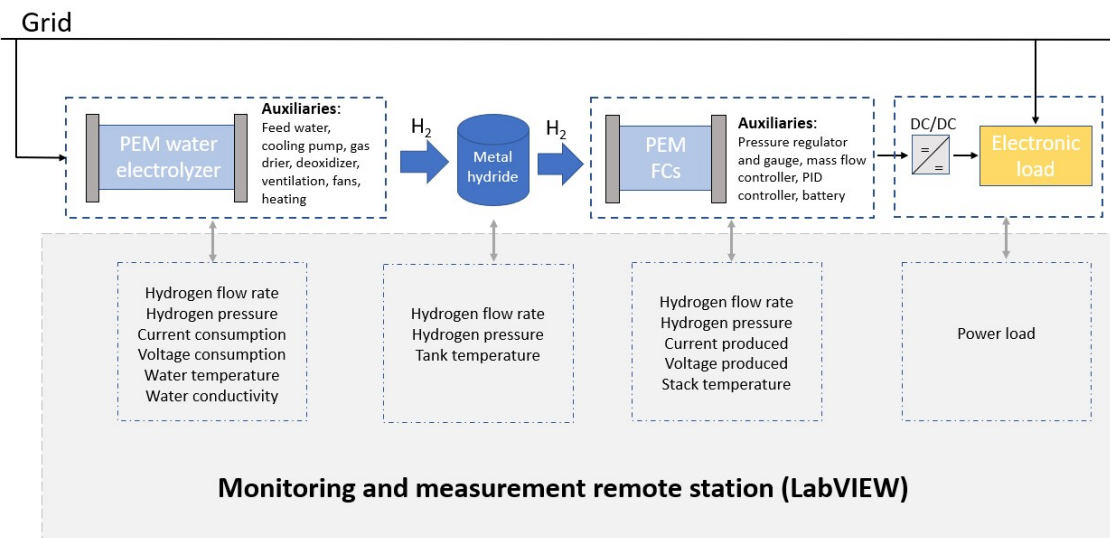

Figure 1. MG layout and monitoring and measurement station

2. Laboratory scale micro-grid

The system includes a PEM water electrolyzer for hydrogen production $(325\,W)$, metal hydride tanks for hydrogen storage (two units, $54\,g$ of hydrogen each, $1.08\,wt\%$), a stack of PEM fuel cell for hydrogen conversion in electricity $(200\,W)$, batteries and an electronic load to emulate different operating conditions of the final user. Moreover, the auxiliary systems required for the proper operation of the hydrogen based ESS are present: mass flow controllers, chiller, DC/DC converters, fans, pressure gauges and pressure reducer, gas detection, etc. The RES electricity production is simulated by imposing a variable current to the electrolyser and the batteries by using a LabVIEW script to the system controller. Table 1 lists the main equipment's specifications while Figure 1 shows a sketch of the whole system.

Table 1. Equipment's specifications of micro-grid

System component	Rated capacity	Manufacturer
Electronic load	$7.2\,kW$	Elektro Automatik
PEM Electrolyzer	$325\,W$, $720\,mL/min$	H2Planet
Metal hydride tank	$600\,L$, $30\,bar$	H2Planet
Stack PEM FCs	$200\,W$	Horizon FC
Lead acid batteries	$18 \div 100\,Ah$	RS PRO
Mass flow controller	$20\,NL/min$	Bronkhorst
DC/DC converter	$200\,W$, $24\,V$	XP Power
Chiller	$-40 \div 30\,°C$	Julabo

### 2.1. Measuring and monitoring station

A measuring and monitoring station, developed with the software LabVIEW, controls, collects and classifies all the most important parameters of the devices in an easy way. It manages the electrolyzer, the mass flow controller, installed before the fuel cells and the electronic load too by simulating a load curve. The most important benefits of the measuring station are that it consists in a tool able to switch on and off all the instruments via boolean controllers, to check through LED indicators which devices are running, to modify operating parameters and easily collect them on a single platform both in form of plots and tabs.

The general interface (front panel) is scheduled in tabs through the Tab controls function [8]. Each tab is associated to a single micro-grid device through an appropriate code (block diagram). This arrangement allows to add new devices without changing the other tabs so giving modularity to the system. Figure 2 shows the front panel of electronic load, the electrolyzer and the mass flow controller (MFC).

All the indicators and controllers are grouped and compacted into clusters to facilitate monitoring operations. For each device, four clusters were created for the following purposes:

 a. the remote connection with the instrument;

 b. error tracking;

 c. monitoring and management operations;

 d. saving data.

In addition, the system is also able to communicate and interact with devices having different communication protocols and setting controllers (VISA, Node, Baud Rate, Port, Adress). In
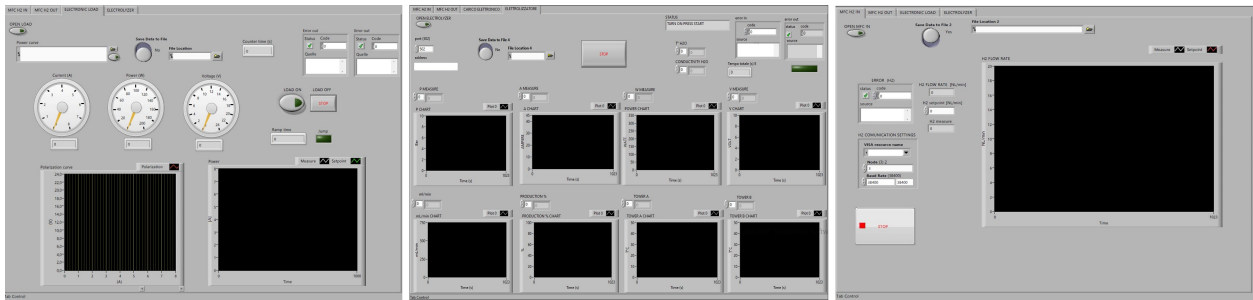
Figure 2. Front panel of devices

fact, the mass flow controllers and the electronic load need an EIA RS 232 protocol, the electrolyzer is connected via Modbus TCP/IP. The operating parameters are reported real time via graphs, numerical indicators and pointer indicators (as shown in Figure 2).

The mass flow controller along with measuring the inlet hydrogen flow, sets the value of flow on a specific setpoint value. This control, once the optimal flow rate for the stack has been identified, will optimize the hydrogen consumption thus increasing the performance.

The communication with the electrolyzer is characterizated by three steps:

1. *created TCP master* function: it allows the communication between the software and the device;
2. *write and read multiple holding registers* function: it transmits the information set into the front panel to the device;
3. *shutdown* function: it closes the communication.

All of those functions are accessed through the Modbus library in LabVIEW [9]. Once the communication with electrolyzer is successful, the station monitors in real time the following parameters: pressure, hydrogen flow rate production and its temperature, the power absorbed by the electrolytic cell, the temperature and conductivity of the water. In particular, the data regarding the cell voltage can be useful to study the degradation phenomena of the cell over time [10].

A specific code fragment was designed for feeding the electronic load with a load profile from an Excel file. The code opens and extracts the values of the Excel file using the *read delimited spreadsheet function* [8]: the Excel file contains the load profile over the time, in particular the first row contains load values (power required) while the second row reports the time.

The data backup can be activated through a boolean controller knob while a path controller is adopted for the location of the saved file. The sampling time has been recreated with the *wait until next ms multiple* function and two shift registers inside a while loop case [8].

3. Methodology for components
The approach used for the characterization of hydrogen devices is described in the following sections.

3.1. Electrolyzer characterization
The hydrogen is produced using a PEM water electrolyzer that dissociates water into hydrogen and oxygen gases. Compared to alkaline electrolyzer, the PEM electrolyzer is a promising technology for high pure efficient hydrogen production from RES thanks to its high current density, high efficiency, faster dynamic response, lower derating for intermittent use and wider operating power ranges. However, its high cost of components makes it more expensive [11].

For the selected electrolyzer, the water must be bidistilled with conductivity below $0.2\,\mu S/cm$. The produced hydrogen can achieve a maximum pressure of $10\,bar$, and a high degree of purity (UPH), without any purification system. The gas generation process is completely controlled by a programmable logic controller (PLC) developed by manufacturer and allows operation at currents up to $45\,A$, whose hydrogen production is $720\,mL$ per minute. The hydrogen produced at $10\,bar$ is not further compressed.

According to guidelines in [12], the polarization curve and efficiency of the electrolyser has been experimentally evaluated. The polarization curve represents the relationship between voltage and current in the electrolyzer from its activation up to the achievement of rated value of hydrogen flow rate $(45\,A)$ while the electrolysis efficiency is calculated through the following equation:

$$\eta_{el} = \frac{\dot{m}_{el}\,LHV}{P_{el}} \tag{1}$$

where $P_{el}\,[W]$ is the electrical power absorbed by the electrolytic cells inside the electrolyzer, $\dot{m}_{el}\,[kgs^{-1}]$ is the hydrogen flow rate produced by the electrolyzer and $LHV\,[Jkg^{-1}]$ is the lower heating value of hydrogen.

3.2. Stack fuel cells characterization

The PEM fuel cell converts hydrogen and oxygen into water and electricity. The stack used in this work has 40 cells and a rated power of $200\,W$. A PID controller manages the stack temperature, blowers, hydrogen input, purging and short circuiting of the stack. The stack operates in passive mode, which means that the air flow is due to the natural convection and not driven by a compressor.

The characterization of the device is carried out following the guidelines in [12]. The performance of the stack is characterized using three measurements: stack polarization curve, hydrogen consumption and efficiency. For the polarization curve, data obtained were compared with those provided by the manufacturer and it is obtained by increasing the current demanded of $0.5\,A$ every three minutes. The rate of hydrogen consumption is proportional to the current, according to the Faraday's law, as it is shown in the following expression [13]:

$$N_{H_2} = \frac{I\,n}{2\,F} \tag{2}$$

where $N_{H_2}\,[mols^{-1}]$ is the consumed hydrogen, $I\,[A]$ is the stack current, n is the number of cells and $F\,[Cmol^{-1}]$ is the Faraday constant.

This data is compared with the real hydrogen flow rate at the inlet, which is detected from mass flow controller installed before the stack. Consequently, the utilization factor, expressing the amount of hydrogen involved in the reaction respect than the flow rate at the inlet, is calculated as follows [14]:

$$UF = \frac{\dot{m}_{H_2react}}{\dot{m}_{H_2in}} \tag{3}$$

where $\dot{m}_{H_2react}\,[Lmin^{-1}]$ is the hydrogen reacted flow rate and $\dot{m}_{H_2in}\,[Lmin^{-1}]$ is the hydrogen inlet flow rate measured by the mass flow controller.

Finally, the stack efficiency is calculated by following equation:

$$\eta_{stack} = \frac{P_{EL}}{\dot{m}_{H_2in}\,LHV} \tag{4}$$

where $P_{EL}\,[W]$ is the electrical power delivered by the stack.

3.3. Metal hydride characterization

The hydrogen produced via electrolysis is stored in a metal hydride system. Unlike physical hydrogen storage technologies (pressure or cryo-compressed), hydride technology allows hydrogen to be stored at the atomic level and in a solid-gaseous system. The operating pressure is thus lower than pressured systems, with the advantage of being safer [15]. The efficiency of these systems is strongly influenced by the need of energy to promote the reactions of absorption and desorption of hydrogen even if it is generally higher than the energy efficiency of the process of liquefaction of hydrogen [16]. The most important issue that penalizes this type of storage is the high weight of the materials even if the problem is limited for stationary applications (as for the micro-grid).

The specific hydrogen storage is based on commercial AB_2 metal hydrides alloy produced by H2Planet. The enthalpy and entropy variation values of this alloy is provided by Facci et al [17] that estimate the heat generated by the hydrogen absorption and desorption process of a similar AB_2 storage system provided by the same manufacturer. Specifically, such an alloy is characterized by $\Delta h = -14\,kJ/mol$ and by an entropy variation $\Delta s = -64\,J/(mol\,K)$, resulting in an equilibrium pressure of $10\,bar$ (p_{eq}) according to Van't Hoff equation:

$$ln(\frac{p_{eq}}{p_0}) = \frac{\Delta h}{R_u\,T} - \frac{\Delta s}{R_u} \tag{5}$$

where p_0 is the atmosferic pressure and R_u is the universal gas costant.

The heat realeased by absorption cycle is computed by following equation:

$$Q = \frac{m_{el}\,\Delta h}{PM_{H_2}} \tag{6}$$

where $m_{el}\,[g]$ is the hydrogen content in the metal hydrided system and PM_{H_2} is the molecular weight of hydrogen.

Since the stack requires hydrogen at a specified constant pressure, a pressure regulator is connected between the stack and the hydrogen storage system to operate efficiently and safely and to supply hydrogen at constant pressure.

Among several types of measurement methods that can be used to investigate hydrogen storage materials and systems (such as static and dynamic tests) [18], dynamic tests were conducted. Dynamic measurements are characterized by continuous changes in pressure and temperature and do not allow to reach the equilibrium. Although they are not ideal for investigating purely thermodynamic properties, they can provide information on the kinetic activity of a material and they are more useful for evaluating a material's hydrogen storage performance during the operation. When hydrogen flows at a constant rate into a hydrogen storage system, the pressure increases linearly and directly proportional to the quantity of hydrogen stored up to a maximum point. After this point, the pressure increase is a function of the material's ability to sorb hydrogen: the sorbption of hydrogen is only due to the capability of the material to host hydrogen, in fact the pressure remains constant, therefore the flow rate of hydrogen into the tanks is equal to the rate of hydrogen sorbed by the material.

The metal hydride tank is located in a water canister cooled by a chiller. The hydride adsorption is tested at four different temperatures of the water canister $(5, 10, 15, 20\,°C)$ in order to evaluate the duration of charging time, the storaged hydrogen (in mass and respect to the density gravimetric of the system) and the energy consumption (energy absorbed from the electrolyser to produce hydrogen).

4. Experimental results
The experimental data are elaborated and presented in this section.

4.1. Polarization curve of electrolyzer

Figure 3 shows the polarization curve of electrolytic cell. A polynomial regression of the sixth order, with a R^2 of 0.9988, fits the experimental data. At its nominal value, the cell absorbs $45\,A$ with a voltage of $4.1 \pm 0.1\,V$ and so requiring $185 \pm 5\,W$ for the electrolysis process. The electrolysis efficiency reaches $75\,\%$ for low current values and $69.5\,\%$ for high current values with an average efficiency of $72.25\,\%$. The performance of the PEM electrolyzer agrees with the literature where a range of efficiency between $60 \div 80\,\%$ is reported [11].
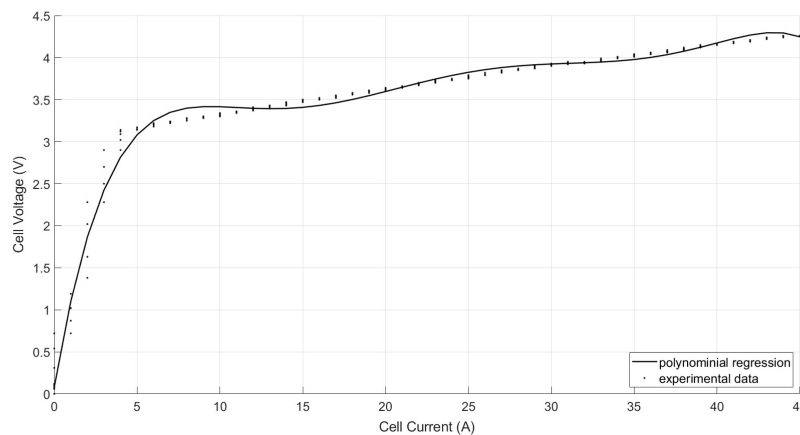
Figure 3. Electrolyzer polarization curve

4.2. Polarization curve of stack

Figure 4 shows the characteristic polarization curve and the power curve of the stack at room ambient temperature, provided by manufacturer, and at $40\,^{\circ}C$, experimentally replicated in laboratory. At ambient temperature, the stack has an open circuit voltage of $38\,V$ and can generate a current up to $9.5\,A$ with a voltage of $20\,V$. At rated power, it generates $8.3\,A$ and $24\,V$ with a stack efficiency of $40\,\%$.

At $40\,^{\circ}C$, the measured stack voltage is lower than corresponding value at $20\,^{\circ}C$ for each current value up to $8\,A$. After $8\,A$, the stack voltage is greater than that at $20\,^{\circ}C$ and a maximum power value of $243\,W$ is measured with a stack current and voltage of $11\,A$ and $22.7\,V$ respectively. The enhanced performance at increasing cell temperatures can be attributed due to the increase of the catalytic activities for hydrogen electro-oxidation and oxygen reduction with increasing cell temperature. However, the ion conductivity of Nafion membrane or Nafion ionomer in the catalyst layers should decrease with an increase in cell temperature, so the ohm polarization loss should decrease. The data plotted showed an opposite trend, the ohmic resistance at $20\,^{\circ}C$ were lower than that at $40\,^{\circ}C$, this can be attributed to the non-activation of the membrane and of the catalyst layer that during the first hours of operation outperform.

The stack efficiency at $40\,^{\circ}C$ is lower than provided at $20\,^{\circ}C$; the values are reported in table 2. For low current, the stack efficiency rises with current increasing up to $4\,A$ where it reaches the maximum value of $37.84\,\%$. For high current from $4\,A$ up to $10\,A$, the stack efficiency lightly falls and reaches an average value of $33\,\%$. Up this value, the efficiency of stack decreases due to the concentration loss, as shown in Figure 4. For this reason, given the low performance and stability of the stack for these current values, it was considered valid to run the stack up to a maximum current of $10\,A$.
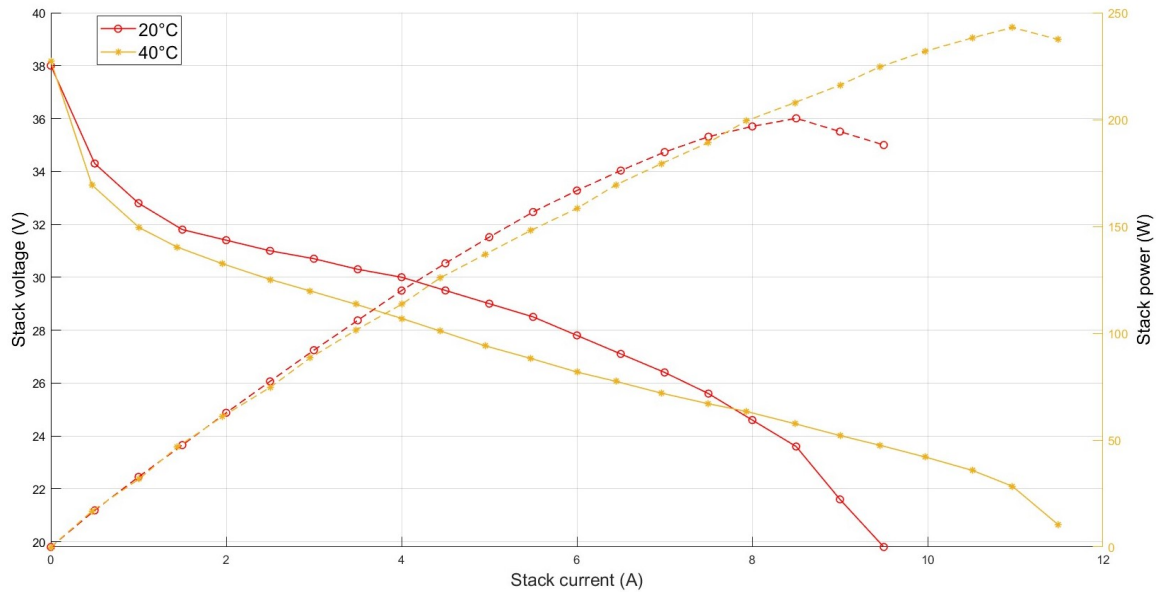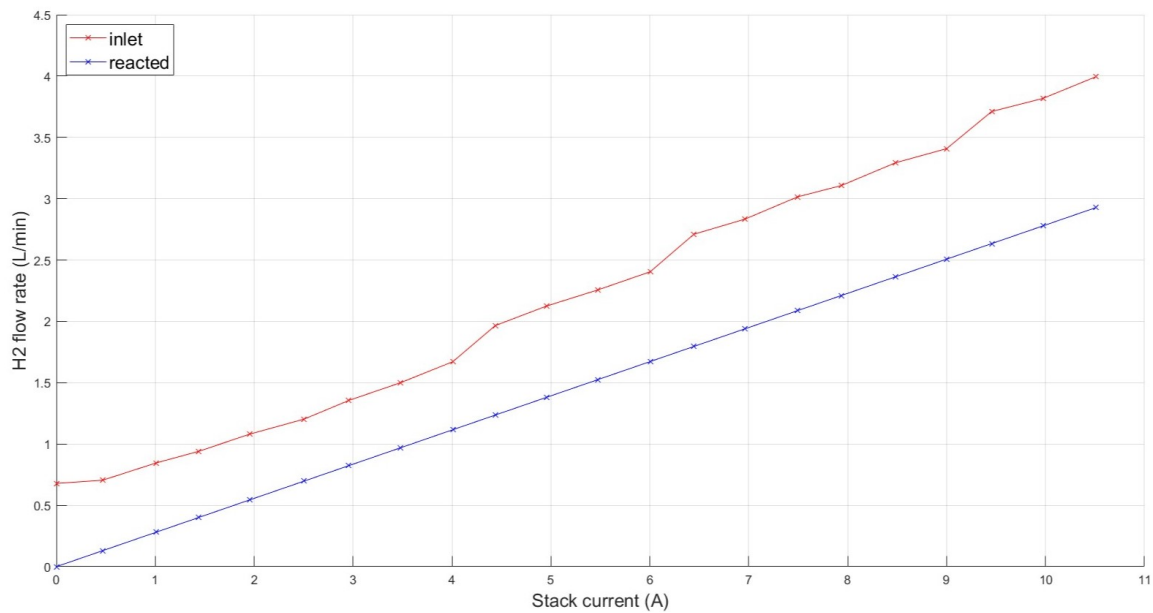
Figure 4. Stack polarization curve

Figure 5. Hydrogen flow at $40°C$

4.3. Hydrogen consumption

Figure 5 shows the hydrogen flow rate when the stack is running at $40\,°C$ focusing on the hydrogen flow rate at the inlet and the reacted one. As shown in table 2, the UF is high and did not show high deviation for current values from $4\,A$ up to $7\,A$ where its average value is about $67.44\,\%$. From $8\,A$ to $10\,A$, UF exceeds $70\,\%$ with an average value of $74.15\,\%$ while from $3\,A$ to $2\,A$ the average value of UF is $55.6\,\%$. The lowest value is under $1\,A$ where is $25.86\,\%$. The farther the working conditions are from the optimum, the lower is the UF. Furthermore,

the results show that at $40\,^\circ C$ the stack works well and stably close to its nominal conditions, in particularly in the range $8 \div 9\,A$. At $10\,A$, the value of UF is the highest but the efficiency is penalized because the fuel cells is working far from the operating conditions.

As here we do not recycle the unreacted hydrogen, this leads to a rapid reduction of the microgrid performance. However, this is just a limit related to the small scales employed. To determine a realistic efficiency value in presence of hydrogen recirculation, in Table 2 the efficiency compared by assuming UF equal 1 (η_{max}), is also reported. The efficiency globally rises, in particular at the nominal condition it increases of $40.56\,\%$, allowing to save the same quantity of hydrogen. The regulation of the hydrogen flow in the inlet to the stack through the mass flow controller, and the eventual recirculation of the hydrogen, will allow to reach the assumed maximum efficiency.

Table 2. Efficiency and UF of the stack at $40\,^\circ C$

Current (A)	1	2	3	4	5	6	7	8	9	10
η (%)	20.93	31.35	36.26	37.84	35.81	36.61	35.16	35.65	35.22	33.75
UF (%)	33.19	50.41	60.77	66.81	64.97	69.55	68.44	71.14	73.56	77.76
η_{max} (%)	63.03	62.19	59.67	56.58	55.11	52.64	51.37	50.11	47.88	46.38

4.4. Metal hydride in charging phase

Figure 6 shows the pressure-gravimetric hydrogen density of the storage tank at four different temperatures $(5, 10, 15, 20\,^\circ C)$.
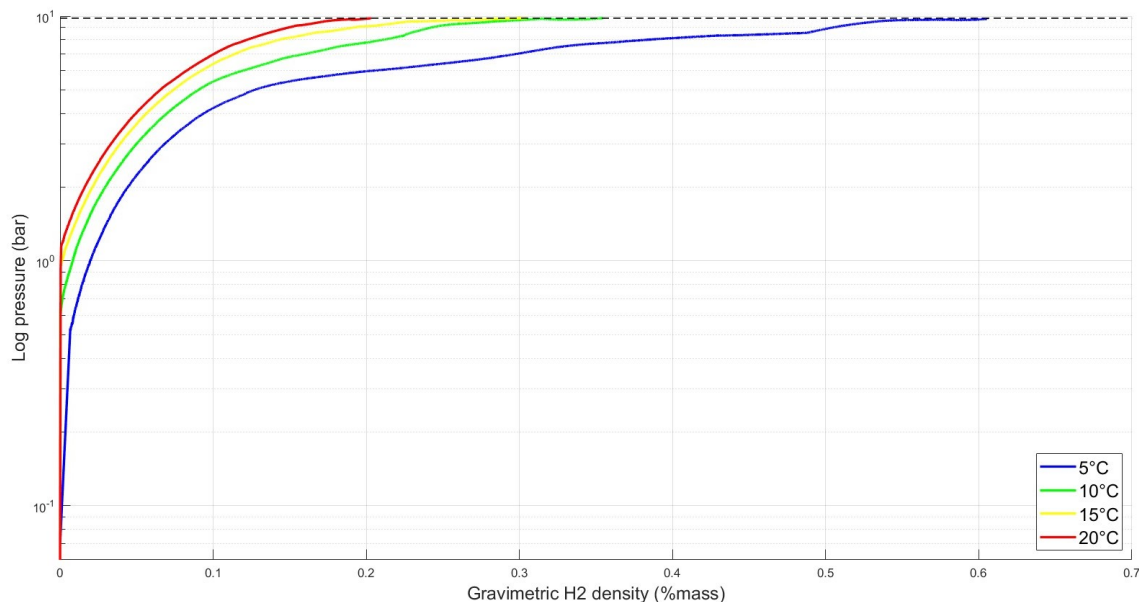
Figure 6. Pressure - Gravimetric H_2 density of metal hydride during the charging phase

The plot showed that a decrease of temperature improved the capability of the material to store hydrogen as the lower temperatures favor the hydride hydrogenation reaction due to its

exothermic nature. In addition, at $5\,°C$ the pressure nearly reached a plateau under a value of $10\,bar$ due to its increasing in the adsorption capacity of the metal hydride. In table 3 the main results obtained during the charging phase at different temperatures are summarized: the gravimetric hydrogen density of the system, the hydrogen content, the duration of charging time, the released heat and the energy consumption of electrolyzer. The maximum hydrogen content ($30.67\,g$) is reached when the storage system is cooled at $5\,°C$ while the minimum content ($10.28\,g$) is obtained at $20\,°C$, according to the thermodynamics of metal hydrides [16]. It is important to point out that the measured values are affected by the lower operative pressure ($10\,bar$) with respect to the nominal maximum pressure of the storage ($30\,bar$). The hydrogen content changes slightly comparing the results obtained at $20, 15, 10\,°C$ while the real gain in hydrogen content is at $5\,°C$. However, an important aspect is the correlation between duration of charging time and hydrogen loading: the percentage increase of the content of hydrogen at $5\,°C$ compared to that at $20\,°C$ is $198\,\%$ higher, but it led to higher operating time ($186\,\%$ higher adopting the same condition). This aspect affects the energy required by the electrolyzer that increases when decreasing the temperature because with the hydrogen content also the charging time greatly rises too. Between 10 and $5\,°C$ the percentage increase is only $16\,\%$ against an increment of time of $22\,\%$.

We must take in mind that, when considering hydrogen storage, the real target is to maximize the hydrogen quantity in the reservoir. It is obvious that storing more hydrogen requires to spend more time and to operate at lower temperature. Nevertheless, this also means operating at higher gravimetric and volumetric efficiency supporting the overcoming of one of the most relevant issues in the hydrogen application. Further research will be carried out in order to find the optimal trade of between operating time and hydrogen loading.

Table 3. Summary results of charging phase

T ($°C$)	Density ($wt\%$)	H_2 content (g)	Charging time (h)	Q (kJ)	E_{el} (kJ)
5	0.605	30.67	8.34	214.7	5331.6
10	0.355	17.92	5.30	125.4	3225.6
15	0.305	15.44	4.32	108.1	2602.8
20	0.202	10.28	2.91	72.0	1742.4

4.5. Micro-grid efficiency

In the micro-grid the hydrogen production-storage and conversion phases are decoupled. The hydrogen production and storage side involves the electrolyzer, the metal hydrides tank to be loaded and its cooling system (a chiller) while the conversion side is composed of the charged metal hydrides tank, the fuel cells, the dc-dc converter and the programmable electronic load. Therefore, two overall microgrid efficiencies for each side are considered: $\eta_{grid,storage}$ for hydrogen production and storage, listed in the Table 4, and $\eta_{grid,user}$ for hydrogen conversion, listed in the Table 5.

In the Table 4, the results for the four tank temperatures (5, 10, 15 and 20 $°C$) are reported. The hydrogen production and storage efficiency of microgrid is the product of the efficiency of electrolyzer and chiller. The electrolyzer efficiency is $69.5 \pm 2\,\%$ as mentioned above while the efficiency of chiller is delivered by manufacturer. Along with this efficiency, a charge efficiency is computed as the ratio between the effective hydrogen content after the charge of metal hydride tank and the maximum hydrogen content ($54\,g$ corresponding a storage pressure of

$30\,bar$). As shown in the Table 4, without compression over $10\,bar$, the hydrogen production and storage efficiency decreases as the temperature unlike the charge efficiency that instead increases. Therefore, the charge efficiency is maximum for $5\,°C$ where is $56.4\,\%$ the hydrogen production and storage efficiency is maximum for $20\,°C$ where it values $67.9\,\%$. Further studies will be carried out in order to storage hydrogen or decreasing the temperature under $5\,°C$ or increasing the storage pressure through the installation of a compressor after the electrolyzer.

Table 4. Hydrogen production and storage efficiency of micro-grid

T_{tank} $(°C)$	η_{charge} $(\%)$	$\eta_{chiller}$ $(\%)$	$\eta_{grid,storage}$ $(\%)$
5	56.8	68.5	47.6
10	33.2	78.3	54.4
15	28.6	88.0	61.2
20	19.0	97.8	67.9

The hydrogen conversion efficiency of the microgrid is computed as the product of the efficiency of stack and dc/dc converter. In the Table 5, the stack efficiency for UF=1 and UF< 1 in the nominal condition ($8\,A$), as listed in the Table 2, are reported. The dc/dc converter efficiency is provided by manufacturer and it is $87\,\%$. In addition, an discarge efficiency is calculated. This is the ratio between the hydrogen quantity consumpted during the discharge and the hydrogen quantity available in the metal hydride container before the discharge. The hydrogen discharge happened in ambient room temperature without warming system. During the discharge, the gaseous hydrogen supplys the fuel cells and the pressure inside the tank decreases. Without a proper warming system, also the metal hydride temperature decreases limiting the desorption flow of hydrogen from metal alloy and thus the hydrogen availability for a specific time period. In the Table 5, two temperatures of hydrogen storage during the charge (5 and $20\,°C$) are considered. The discharge efficiency is higher at $20\,°C$ than at $5\,°C$ because a low temperature the quantity of storaged hydrogen is major and its complete release need warm according to endhotermic nature of the process. Instead, at $20\,°C$ the hydrogen flux involved does not represent a significant quantity and it is indeed negligible from an exergetic point of view and the efficiency is consequently major. However, at $5\,°C$ the discharge time was 1 hour while for $20\,°C$ was 25 minutes. Therefore, at $20\,°C$ the hydrogen conversion efficiency of the microgrid is $19\,\%$, that is $7.34\,\%$ higher than that for $5\,°C$ but the working time of stack is $140\,\%$ minor.

Table 5. Hydrogen conversion efficiency of micro-grid

$\mathbf{T_{charge}{=}5°C}$	η_{stack} $(\%)$	$\eta_{dc/dc}$ $(\%)$	$\eta_{discarge}$ $(\%)$	$\eta_{grid,user}$ $(\%)$
UF= 1	50.1	87.0	57.2	43.6
UF< 1	35.6	87.0	57.2	31.0
$\mathbf{T_{charge}{=}20°C}$	η_{stack} $(\%)$	$\eta_{dc/dc}$ $(\%)$	$\eta_{discarge}$ $(\%)$	$\eta_{grid,user}$ $(\%)$
UF= 1	50.1	87.0	61.3	43.6
UF< 1	35.6	87.0	61.3	31.0

5. Conclusion

In this paper, the characterization of hydrogen devices of a microgrid was carried out through the development of a measurement and monitoring station using the software LabVIEW. The study highlights the importance of the characterization of each device before their integration because it allowed to identify how the devices run, when malfunction occurs so avoiding losing energy and supporting a proper use of equipments. The performance of the electrolytic cell agrees with the literature where an average efficiency of 70% is reported. The fuel cell stack can work stably and continuously in a current range of $3 \div 10\,A$ with an average efficiency of 35% despite the detrimental effect of an UF that is well below the unity. Regarding the influence of temperature on charging phase of the tank, the lower is the temperature the higher is the amount of hydrogen stored and consequently the storage efficiency of the microgrid. To significantly increase the autonomy and the efficiency of the system, in the discharge phase it would be necessary to provide a proper heating system and a recirculation of the unreacted hydrogen. Further studies will be carried out on the system to create a huge data set than can be also used to develop a predictive control framework model and to investigate the combination of the main paramers that will lead an optimum in term of energy performance.

References

[1] Enayatizade H, Chahartaghi M, Hashemian S M, Arjomand A and Ahmadi M H 2019 *International Journal of Low-Carbon Technologies* **14** 170–186
[2] IEA R 2020 *Special Report on Carbon Capture, Utilisation and Storage.*
[3] Hassan I, Ramadan H S, Saleh M A and Hissel D 2021 *Renewable and Sustainable Energy Reviews* **149** 111311
[4] Ulleberg Ø 2004 *Solar Energy* **76** 323–329
[5] Cau G, Cocco D and Petrollese M 2014 *Energy Procedia* **45** 12–21
[6] Ulleberg Ø, Nakken T and Ete A 2010 *International journal of hydrogen energy* **35** 1841–1852
[7] Valverde L, Rosa F and Bordons C 2013 *IEEE transactions on industrial informatics* **9** 1398–1404
[8] Bishop R H 1999
[9] Zhan W, Porter J R and Morgan J A 2013 *IEEE Transactions on Education* **57** 34–41
[10] Voronova A, Kim H J, Jang J H, Park H Y and Seo B 2022 *International Journal of Energy Research*
[11] Kumar S S and Himabindu V 2019 *Materials Science for Energy Technologies* **2** 442–454
[12] Harrison K W, Remick R, Hoskin A and Martin G 2010 Hydrogen production: fundamentals and case study summaries Tech. rep. National Renewable Energy Lab.(NREL), Golden, CO (United States)
[13] San Martin J, Zamora I, San Martin J, Aperribay V, Torres E and Eguia P 2010 *Energy* **35** 1898–1907
[14] Baghban Yousefkhani M, Ghadamian H, Daneshvar K, Alizadeh N and Rincon Troconis B C 2020 *Energies* **13** 6117
[15] Rusman N and Dahari M 2016 *International Journal of Hydrogen Energy* **41** 12108–12126
[16] Von Colbe J B, Ares J R, Barale J, Baricco M, Buckley C, Capurso G, Gallandat N, Grant D M, Guzik M N, Jacob I *et al.* 2019 *international journal of hydrogen energy* **44** 7780–7808
[17] Facci A L, Lauricella M, Succi S, Villani V and Falcucci G 2021 *Energies* **14** 1554
[18] Gross K J, Carrington K R, Barcelo S, Karkamkar A, Purewal J, Ma S, Zhou H C, Dantzer P, Ott K, Pivak Y *et al.* 2016 Recommended best practices for the characterization of storage properties of hydrogen storage materials Tech. rep. EMN-HYMARC (EMN-HyMARC); National Renewable Energy Lab.(NREL)